The following publication J. Zhou, J. Lu, G. Zhou and C. Lu, "Joint OSNR and Frequency Offset Estimation Using Signal Spectrum Correlations," in Journal of Lightwave Technology, vol. 39, no. 9, pp. 2854-2863, 1 May 2021 is available at https://doi.org/10.1109/JLT.2021.3063251.

Joint OSNR and Frequency Offset Estimation Using Signal Spectrum Correlations

Jing Zhou, Jianing Lu, Gai Zhou, and Chao Lu, *Fellow, OSA*

***Abstract*— We propose an efficient and modulation-format-transparent method to jointly estimate optical signal-to-noise ratio (OSNR) and frequency offset (FO) by using signal spectrum correlations for coherent optical fiber communication systems. Based on the signal spectrum correlation analysis, a coarse FO estimation (FOE) and the corresponding compensation can be conducted after chromatic dispersion compensation (CDC). Then, OSNR monitoring can be accurately operated without deterioration caused by FO. Meanwhile, to realize fine FOE, down-sampling process of signal can be used to reduce the complexity of fast Fourier transform-based FOE (FFT-FOE) without losing FOE resolution. Simulation results show that when the OSNR is in the range of 10dB to 30dB, the proposed scheme presents an absolute OSNR estimation error lower than 0.18 dB. Finally, we experimentally demonstrate our scheme in an optical back-to-back (B2B) transmission link using 28 Gbaud dual-polarization (DP)-4/16/32-quadrature amplitude modulation (QAM) formats, and an absolute OSNR estimation error lower than 0.66 dB is achieved for OSNR ranging from 15 dB to 30 dB.**

***Index Terms*—Coherent communications, optical fiber communication, optical performance monitoring.**

I. Introduction

As one of the key indicators of optical signal quality, optical signal-to-noise ratio (OSNR) needs to be accurately monitored to guarantee the performance of coherent optical communication systems [1, 2]. For next-generation heterogeneous and flexible optical networks, there exist a number of different optical path links and modulation formats [3, 4]. Therefore, an efficient and modulation format-transparent optical performance monitoring (OPM) technique becomes highly desirable to adapt and handle complicated link conditions [5]. With the help of OPM, the network operators can evaluate the quality of transmission (QoT) and take possible measures according to monitored OSNR value.

Various types of OSNR monitoring schemes have been proposed so far. Conventional out-of-band interpolation method [6] measures the power of signal and amplified spontaneous emission (ASE) noise in optical spectrum to calculate OSNR. However, it is not suitable for dense wavelength division multiplexing (WDM) systems with the presence of reconfigurable optical add-drop multiplexers (ROADMs) [7]. Instead, it is more desirable to employ in-band OSNR monitoring for state-of-the-art coherent communications systems [3]. Thanks to the development of digital signal processing (DSP) techniques, one can perform noise analysis in electrical domain [8]. Since the information of OSNR is reflected in electrical SNR (ESNR), which can be analyzed and calculated by DSP algorithms, a number of DSP-based OSNR monitoring methods have been proposed. For example, ESNR can be directly obtained by error vector magnitude (EVM) calculation after complete DSP flow [9]. Meanwhile, Stokes-vector [10] and statistical moments [11] based methods have also been analyzed. Among DSP-based OSNR monitoring techniques, cyclostationary property of the signal has been analyzed and applied to OSNR monitoring which separates the pure signal power out from the whole received power to calculate the SNR [12]. However, the performance degrades for high OSNR conditions. Another cyclostationary property-based OSNR estimation method is proposed in [13], where correlation between two spectral components at the upper and lower sideband of the signal spectrum is used to calculate the OSNR. Although this method is insensitive to modulation formats, polarization rotation, polarization mode dispersion (PMD), and DSP-induced noise, its performance degrades significantly in the presence of FO, as analyzed in Section II.

FO is induced by wavelength mismatch of transmitter laser and the local oscillator (LO). Several FO estimation (FOE) schemes have been proposed for single carrier systems [14–17]. The differential FOE (Diff-FOE) estimates FO by computing the phase increment between two adjacent symbols raised to the 4^{th} power for quadrature amplitude modulation (QAM) format [16, 17]. Another popular FOE is fast Fourier transform-based FOE (FFT-FOE) [14, 15], where the peak of the 4^{th} power signal spectrum is searched to locate the FO value. Although FFT-FOE may work well directly after chromatic dispersion compensation (CDC) at high OSNR conditions [18], these two FOE methods are both better to be operated after polarization demultiplexing and inter-symbol-interference mitigation to guarantee the performance. For above-mentioned signal spectrum correlation-based OSNR monitoring scheme, the FO is required to be corrected immediately after CDC, limiting the use of Diff-FOE and FFT-FOE. On the other hand, for future ultra-dense WDM with advanced signal spectrum arrangement, such as subcarrier-multiplexing [19, 20] and faster-than-Nyquist systems [21], it is necessary to correct the FO before signal-

This work was supported in part by the National Key R&D Program of China (2018YFB1801701), National Natural Science Foundation of China (NSFC) (U1701661 and 61435006), and Hong Kong PhD Fellowship Scheme (HKPFS). (*Corresponding author: Jianing Lu*)

J. Zhou, J. Lu, and C. Lu are with the Photonics Research Centre, Department of Electronic and Information Engineering, The Hong Kong Polytechnic University, Hong Kong (e-mail: jing-dv.zhou@connect.polyu.hk; jianing.lu@connect.polyu.hk; chao.lu@polyu.edu.hk). C. Lu is also with The Hong Kong Polytechnic University Shenzhen Research Institute, Shenzhen 518057, China.

G. Zhou is with Department of Electrical Engineering, The Hong Kong Polytechnic University, Hong Kong (e-mail: gai.zhou@connect.polyu.hk).

demultiplexing filtering. Therefore, FOE operated at an earlier stage of DSP flow is worthy of further study.

In this paper, we propose a joint OSNR and FO estimation scheme using signal spectrum correlations for coherent optical fiber communication systems. Inspired by characteristics of flat linear noise spectrum, we carry out a semi-analytical investigation on the impact of FO on the correlation value between two spectral components at the upper and lower sideband of the signal spectrum. We propose to conduct FO sweeping of signal with optimized FO range and step size. Then, corresponding correlation values are calculated. FO value is estimated by quadratic curve fitting of the relation between swept FO values and correlation values. The obtained estimated FO value can be used to carry out coarse FO compensation (FOC), after which we can conduct accurate OSNR monitoring with compensated signal using correlation calculations-based method [13]. Meanwhile, down-sampling process of signal can be used to reduce the complexity of FFT-FOE while keeping high FOE resolution at fine FOE stage. Such joint OSNR and FO estimation structure not only guarantee the OSNR monitoring performance, but also optimize the overall efficiency. Simulation results show that the proposed scheme can accurately monitor OSNR within absolute estimation error lower than 0.18 dB within the OSNR range of 10 dB-30 dB while the monitoring error performance without FOC becomes unacceptable. Finally, performance of our proposed scheme is experimentally verified under the scenario of optical back-to-back (B2B) transmission using 28 Gbaud dual-polarization (DP)-4/16/32-QAM formats with absolute OSNR estimation error lower than 0.66 dB within the OSNR range of 15 dB-30 dB.

II. Analysis of Impact of FO on Cyclostationary Property-Based OSNR Monitoring Scheme

A. Belief introduction of cyclostationary property-based OSNR monitoring scheme

Our proposed joint OSNR and FO estimation scheme is based on a classical cyclostationary property-based OSNR estimation method [13]. Therefore, we first give a belief introduction of the basic principle of this method. Previously, cyclostationary property of digitally modulated signal has been comprehensively studied in [22, 23]. For common digital modulation formats, such as phase-shift keying (PSK) and QAM, since their symbol durations are predetermined and time-invariant, there is distinct difference between the statistical property of signal and that of Gaussian noise. The 1st and 2nd order statistical properties (i.e. the mean value and autocorrelation function) are defined as:

$$\bar{\mu}_m = E[m(t)] \tag{1}$$

$$\bar{R}_m(\tau) = E[m(t+\frac{\tau}{2})\cdot m^*(t-\frac{\tau}{2})] \tag{2}$$

where $m(t)$, $\bar{m}$ and m^* represent the signal, the estimated value and the complex conjugate of m, respectively, and E is the expectation operator. It is obvious that the mean values of signal and ASE noise are both zero. On the contrary, $\bar{R}_m(\tau)$ is periodic in time at periodic interval of symbol duration T_s, as long as τ is less than T_s, while autocorrelation function of ASE noise does not exhibit such periodicity [22]. In the signal spectrum, the periodicity of $\bar{R}_m(\tau)$ exhibits strong correlations between time-varying amplitude and phase sequences of certain pairs of spectral components, while such correlations do not exist for ASE noise. A spectral correlation density function (SCDF), $S_m^{\alpha}(f)$, is defined to describe correlations between spectral components of signal. $S_m^{\alpha}(f)$ is defined as the Fourier transformation of the cyclic autocorrelation function [22], $R_m^{\alpha}(\tau)$, of the time-varying signal sequence $m(t)$, as

$$R_m^{\alpha}(\tau) \equiv E[m(t+\tau/2)\cdot m^*(t-\tau/2)\cdot\exp(-j2\pi\alpha t)] \tag{3}$$

and $S_m^{\alpha}(f)$ is

$$S_m^{\alpha}(f) \equiv \int_{-\infty}^{\infty} R_m^{\alpha}(\tau)\cdot\exp(-j2\pi f\tau)d\tau \tag{4}$$

The SCDF can also be expressed as a correlation function of the time-varying amplitudes of different spectral components equivalently, as

$$S_m^{\alpha}(f) \equiv E[M_T(t, f+\alpha/2)\cdot M_T^*(t, f-\alpha/2)] \tag{5}$$

where

$$M_T(t,v) = \int_{t-T/2}^{t+T/2} m(u)\cdot\exp(-j2\pi vu)du \tag{6}$$

T is integration time much larger than T_s. The normalized SCDF can be expressed as

$$\hat{S}_m^{\alpha}(f) \equiv \frac{E[M_T(t, f+\alpha/2)\cdot M_T^*(t, f-\alpha/2)]}{\sqrt{E[|M_T(t, f+\alpha/2)|^2]}\sqrt{E[|M_T(t, f-\alpha/2)|^2]}} \tag{7}$$

For noiseless digital modulated signals, theoretically, $\hat{S}_m^{\alpha}(f)$=1 when $\alpha=\alpha_0=1/T_s$ and for all f within [$-\alpha/2, \alpha/2$], as long as two frequencies $f-\alpha_0/2$ and $f+\alpha_0/2$ are within the bandwidth of the modulated signal. On the contrary, there is no significant correlation between spectral components of ASE noise which is a random Gaussian process. At the receiver, the optical signal will be mixed with ASE noise induced by optical amplifiers, making $\hat{S}_m^{\alpha_0}(f)$ smaller than 1. Considering n be the ASE noise, we have the following Fourier transform relation:

$$\begin{aligned}\tilde{M}_T(t,v) &= \int_{t-T/2}^{t+T/2}(m(u)+n(u))\cdot\exp(-j2\pi vu)du \\ &= M_T(t,v)+N_T(t,v)\end{aligned} \tag{8}$$

Then, the normalized SCDF can be expressed as

$$\hat{S}_m^{\alpha}(f) = \frac{E[M_T(t, f+\alpha/2)\cdot M_T^*(t, f-\alpha/2)]}{\sqrt{E[|M_T(t, f+\alpha/2)|^2+|N_T(t, f+\alpha/2)|^2]}\cdot\sqrt{E[|M_T(t, f-\alpha/2)|^2+|N_T(t, f-\alpha/2)|^2]}} \tag{9}$$

Here, for the numerator, $E[M_T(t, f+\alpha/2)\cdot N_T^*(t, f-\alpha/2)]$ and $E[N_T(t, f+\alpha/2)\cdot M_T^*(t, f-\alpha/2)]$ are cross items of signal and noise, while $E[N_T(t, f+\alpha/2)\cdot N_T^*(t, f-\alpha/2)]$ is pure noise items. They are obviously all zero for all $\alpha>0$. Let $f=f_c$, where f_c is the carrier frequency. Since the power

spectra of aforementioned digital formats are symmetric about f_c, then

$$E[|M_T(t, f_c+\alpha/2)|^2]=E[|M_T(t, f_c-\alpha/2)|^2] = E[P_M(f_c \pm \alpha/2)] \quad (10)$$

Meanwhile, the power density of ASE noise is flat over the whole spectrum. Then

$$E[|N_T(t, f_c+\alpha/2)|^2]=E[|N_T(t, f_c-\alpha/2)|^2] = E[P_N(f_c \pm \alpha/2)] \quad (11)$$

where P_M and P_N are power of signal and noise, respectively. The normalized SCDF with $\alpha=\alpha_0=1/T_s$ becomes

$$\hat{S}_m^{\alpha_0}(f_c)=\frac{E[P_M(t, f_c \pm \alpha_0/2)]}{E[P_M(t, f_c \pm \alpha_0/2)]+E[P_N(t, f_c \pm \alpha_0/2)]} \quad (12)$$

Then, the SNR at $f_c \pm \alpha_0/2$ can be expressed as

$$SNR(f_c,\ \alpha_0)=\frac{E[P_M(t, f_c \pm \alpha_0/2)]}{E[P_N(t, f_c \pm \alpha_0/2)]}=\frac{\hat{S}_m^{\alpha_0}(f_c)}{1-\hat{S}_m^{\alpha_0}(f_c)} \quad (13)$$

Considering the OSNR calculation, it needs to consider the whole signal power within the measurement bandwidth B_{meas}, which is equal to the signal bandwidth $\text{Symbol rate}\times(1+\text{ROF})$ and noise power within the reference bandwidth B_{ref} =0.1 nm. Then, OSNR can be expressed as

$$OSNR=\frac{\sum_{f_i \in B_{meas}} E(P_M(f_i)+P_N)}{E(P_M(f_c \pm \alpha_0/2)+P_N)\cdot B_{ref}}\cdot\frac{1}{1-S_m^{\alpha_0}(f_c)}-\frac{B_{meas}}{B_{ref}} \quad (14)$$

where f in $P_N(t)$ is omitted due to the spectral flatness of ASE noise. According to Eq. (14), the OSNR estimation can be efficiently realized by a few simple steps:

(1) Measure the power of the whole received signal within B_{meas}, i.e. $\sum_{f_i \in B_{meas}} E[P_M(t, f_i)+P_N(t)]$.

(2) Use a pair of narrowband filters with center frequency at $f_c-\alpha_0/2$ and $f_c+\alpha_0/2$ to filter out two spectral components, as illustrated in Fig. 1(a). Measure the power of these two spectral components and scale it according to the relative size of B_{ref} and the bandwidth of narrowband filters. Then we obtain $E[P_M(t, f_c \pm \alpha_0/2)+P_N(t)]\cdot B_{ref}$.

(3) Calculated $\hat{S}_m^{\alpha_0}(f_c)$ using two spectral components obtained in step (2). In time domain, after filtering, we obtain two time-varying sequences whose FFT transforms are two spectral components located at $f-\alpha_0/2$ and $f+\alpha_0/2$. Therefore, complicated steps from Eq. (5) to Eq. (7) can be simplified by direct time domain correlation calculation between above-mentioned two filtered time-varying sequences.

Fixing the bandwidth of narrowband filters at 100 MHz [13], the normalized SCDF and the OSNR estimation performance is plotted in Fig. 1(b).

The correlation calculations-based OSNR method is modulation format-transparent since only spectrum information is used without the need of demodulation by complicated DSP. It should be noticed that CDC is essential to avoid correlation degradation induced by time delay between the two spectral components. Meanwhile, benefiting from "quasi-DSP free" feature, DSP-induced noise and the impact of residual phase noise are avoided [8, 24] and the linear fit process between OSNR and ESNR suffers less interference [3]. In contrast, conventional DSP-based OSNR monitoring techniques (e.g. EVM method [9] and statistical moments based method [25, 26]) depend significantly on the DSP performance and are modulation format-dependent. Another advantage of the correlation calculations-based OSNR method is that its performance is insensitive to random rotation in the polarization state and polarization mode dispersion (PMD) in polarization division multiplexing systems. Moreover, this method is insensitive to the laser linewidth induced phase noise.

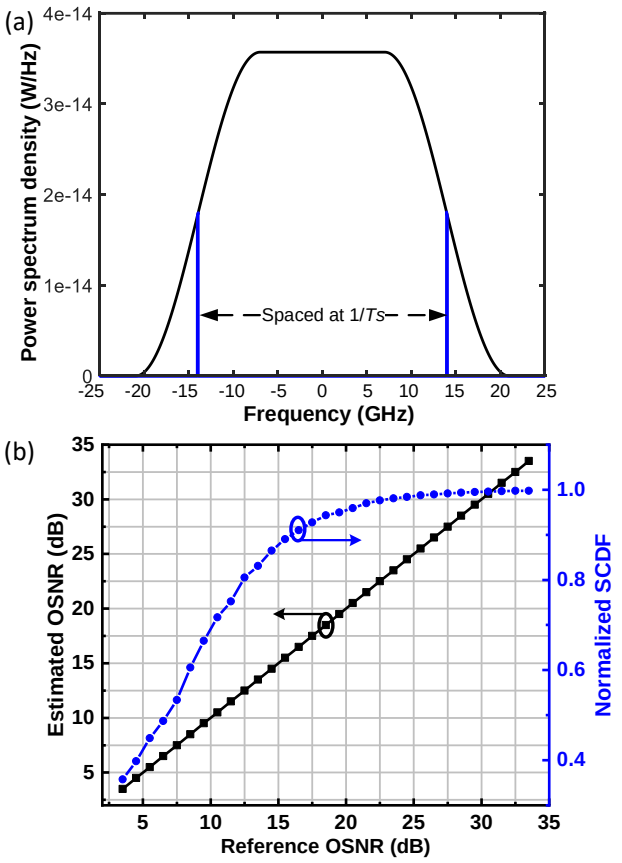

Fig. 1. (a) A power spectrum of 28 GBaud 16-QAM signal and spectral components used for measuring the correlation value spaced at 28G. Signal power is 0 dBm and the roll-off factor (ROF) is 0.5. (b) The normalized SCDF calculated using two spectral components in (a), and the estimated OSNR from the SCDF versus reference OSNR.

B. Impact of FO on OSNR estimation using signal spectral correlation

According to analysis in [22], $\hat{S}_m^{\alpha}(f)=1$ when $\alpha=\alpha_0=1/T_s$ and for all f within $[-\alpha/2, \alpha/2]$. In practice, it should be noticed that in digital optical communications, the bandwidth of a signal is shaped by both electrical and optical filters (e.g. raise-cosine filter, anti-aliasing filter, limited bandwidth of electronic or optics devices) to limit the occupied bandwidth.

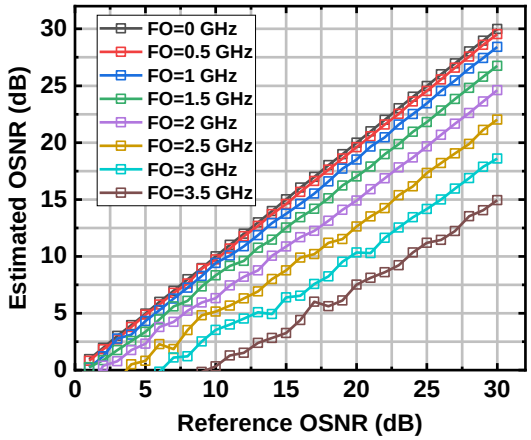

Fig. 2. OSNR estimation performance under various FO from 0 to 3.5 GHz.

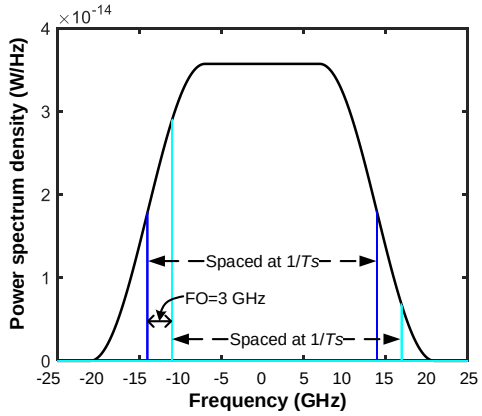

Fig. 3. Position moving process of the two spectral components at the upper and lower sideband with induced-FO of 3 GHz. The signal parameter is same as that in Fig. 1(a).

Therefore, at the receiver side, $\hat{S}_m^{\alpha}(f)$=1 holds under a slightly more stringent condition: Two frequencies $f-\alpha_0/2$ and $f+\alpha_0/2$ should be within the bandwidth of the modulated signal, when the signal is noiseless. According to above analysis, it seems that, the OSNR estimation performance is insensitive to FO as long as frequencies $f-\alpha_0/2$ and $f+\alpha_0/2$ do not exceed the signal bandwidth. However, we have found that in simulation, FO will significantly influence the OSNR estimation performance of signal spectrum correlations-based method under various FO, as shown in Fig. 2. This phenomenon is due to the impact of FO on the correlation value when there exists ASE noise. Let's consider the scenario in the presence of FO and its impact on spectral correlation calculation of a noisy signal. In the correlation measurement steps described previously, for a 28 Gbaud signal, if FO is absent, the ideal situation is to filter out two spectral components at the upper and lower sideband at a frequency of ± 14 GHz which show a central symmetry with the zero frequency. If FO is present, the positions of the two upper and lower sideband signals at the interval of 28 GHz are no longer symmetrical about the center frequency, as shown in the Fig. 3, where we set the FO to be 3 GHz. Here, the effect of FO is equivalently manifested in the position moving of the two narrowband filters instead of that of signal spectrum for convenience. It is worth noting that the power of

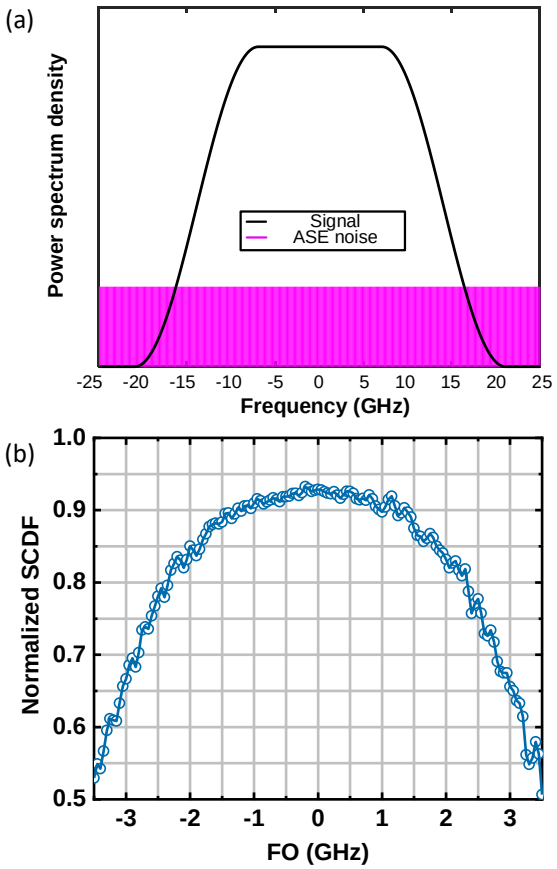

Fig. 4. (a) Signal spectrum of 28 GHz 16QAM signal and ASE noise spectrum. ROF=0.5. (b) An example of relation between normalized SCDF and FO.

two spectral components is no longer the same. Next, let's analyze the impact of FO on the calculation of correlation $\hat{S}_m^{\alpha_0}(f)$. For a noiseless signal, the $\hat{S}_m^{\alpha_0}(f)$ remain theoretically 1 as $\hat{S}_m^{\alpha_0}(f_c)$. It is easy to understand because this process is equivalent to the scenario where there are two identical signals, and one of them is amplified and the other is attenuated. Obviously, $\hat{S}_m^{\alpha_0}(f)$ is still 1 when there is not any noise. But for a signal with flat ASE noise power spectrum density (PSD) as shown in Fig. 4 (a), the situation is quite different. Although the PSD of signal has changed due to its position moving in the spectrum, the PSD of noise is constant cross all frequency. It means that, in the process shown in Fig. 3, the PSD of the spectral component at the upper sideband (on the right of 0 GHz) decreases significantly, and the proportion of noise increases. Although for the lower sideband signal the trend is the opposite, it should be noticed that for the correlation calculation, the result is much more dependent on the noisier component, i.e., the spectral component in the upper sideband in Fig. 3, which causes the drop of $\hat{S}_m^{\alpha_0}(f)$. Therefore, $\hat{S}_m^{\alpha_0}(f)$ decreases with FO as shown in Fig. 4(b).

III. Operation Principle of the Proposed Method

Since the commercially available lasers usually have relatively large FO [27], it is essential to compensate FO of the signal

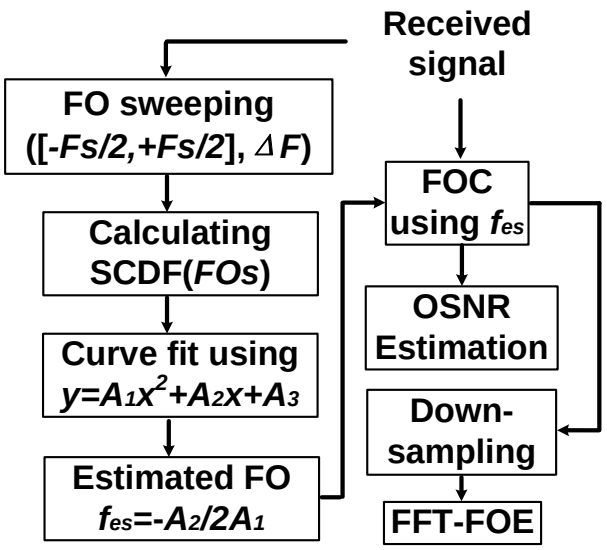

Fig. 5. Schematic of proposed joint OSNR and FO estimation scheme.

before OSNR monitoring to avoid FO-induced performance degradation. According to the analysis in Section II, theoretically, the maximum correlation value is achieved when FO = 0 Hz. Here, we propose to operate FO sweeping on the received signal after CDC. The flow of scheme is plotted in Fig. 5. The signal m with the length of a is swept by an equal frequency spacing of ΔF, over a range of [-Fs/2, +Fs/2],

$$m_h(i)=m(i)\cdot\exp(j\cdot f_h\cdot i) \qquad h=1,2...k, i=1,2...a \tag{15}$$

where $m(i)$ is i^{th} symbol and f_h stands for h^{th} FO within [-Fs/2, +Fs/2] with the equal spacing ΔF. m_h is the signal swept by f_h. Here, sweeping step size ΔF and FO sweeping range should be optimized taking both performance and complexity into account, which will be discussed in Section IV. For each m_h, we calculate corresponding normalized SCDF. Basically, the closer the swept FO is to the FO of the signal, the larger the value of corresponding normalized SCDF $\hat{S}_{m,h}^{\alpha_0}(f)$ is. Therefore, we can realize FO estimation according to the curve of $\hat{S}_{m,h}^{\alpha_0}(f)$ versus f_h. The most direct method is to search f_h at which $\hat{S}_{m,h}^{\alpha_0}(f)$ achieve its maximum value. However, this method only considers the information of the maximum value of $\hat{S}_{m,h}^{\alpha_0}(f)$ and will have relatively larger estimation error. To make use of the sequence of swept FOs and corresponding $\hat{S}_{m,h}^{\alpha_0}(f)$ values as full as possible, we propose to employ curve fitting method in the form of quadratic function, i.e. the relationship between f_h and $\hat{S}_{m,h}^{\alpha_0}(f)$ is obtained through curve fitting using $y=A_1x^2+A_2x+A_3$. For curve fitting, we use the data points of $\hat{S}_{m,h}^{\alpha_0}(f)$ whose difference with max($\hat{S}_{m,h}^{\alpha_0}(f)$) is smaller than a pre-defined threshold (Th). This limit is used to guarantee the quality of the data used for curve fitting. The estimated FO value f_{es} can be specified as the location of symmetrical axis of the fitted quadratic function, which can be expressed as $-A_2/2A_1$. Figure 6 shows an example of FO

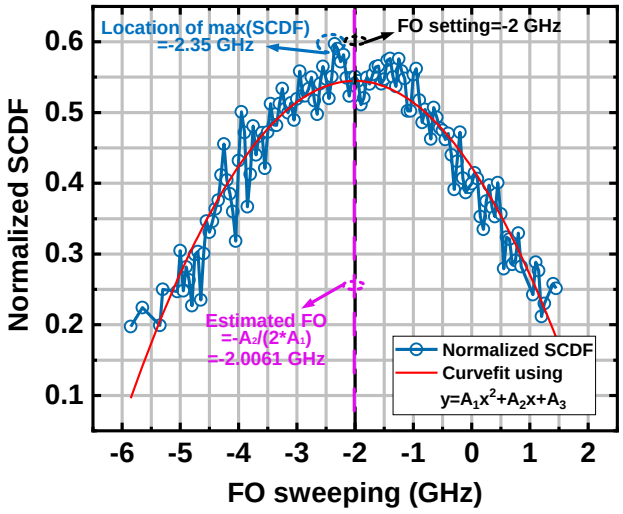

Fig. 6. An example case of FO estimation using maximum value searching method and quadratic function curve fitting method. The FO is set to -2 GHz.

estimation with FO of -2 GHz, while both maximum value searching method and quadratic function curve fitting method are considered. When maximum value searching method is used, it is observed that due to the random fluctuation of the curve, the FOE value is located at -2.35 GHz. On the contrary, with our proposed quadratic function curve fitting method, the FOE value is -2.0061 GHz, which is much more accurate than that of maximum value searching method. After FOC using the estimated FO value, the signal spectrum correlations-based OSNR method is performed. Although at this stage, the coarse FOC is not accurate enough for signal demodulation, it limits the possible FO range to a small range and we can perform signal down-sampling to reduce the complexity of the fine FOE stage after equalization. For fine FOE stage, FFT-FOE is utilized to reduce the residual FOE error, which is essential to guarantee the performance of carrier phase recovery (CPR) [16, 17]. FOE value $\Delta\hat{f}$ of FFT-FOE is calculated by

$$\begin{aligned}\Delta\hat{f} &= \frac{1}{4}\cdot\frac{1}{TN}\arg\max_{k,|k|\le N/2}|F_4(f)| \\ &= \frac{1}{4}\cdot\frac{1}{TN}\arg\max_{k,|k|\le N/2}\left|\sum_{n=0}^{N-1}m^4(n)e^{-j\frac{2\pi nk}{N}}\right|\end{aligned} \tag{16}$$

where $F_4(f)$ is the Fourier transform of 4$^{\text{th}}$ power of signal, $m^4(n)$. N is the length of the signal (also the FFT size). Eq. (16) is realized by FFT [14]. Due to the 4$^{\text{th}}$ power transformation, the FOE range of FFT-FOE is $[-\alpha_0/8,+\alpha_0/8]$ with the resolution of $\alpha_0/4N$. Generally, a proper FFT size is chosen to limit the complexity while keeping a fine FOE resolution. However, since the possible FO range is limited to $\pm\max(abs(\text{coarse FOE error}))$, we can perform down-sampling process of signal with coarse FOC to reduce required FFT size. From the perspective of time domain, the down-sampling process of signal is equivalent to the reduction of the estimation range of FFT-FOE, since the phase difference between two adjacent symbols is multiplied. However, the FOE resolution remains unchanged because FFT size (signal length N) is reduced at the same time. After down-sampling the signal with a down-sampling rate of q, the FOE

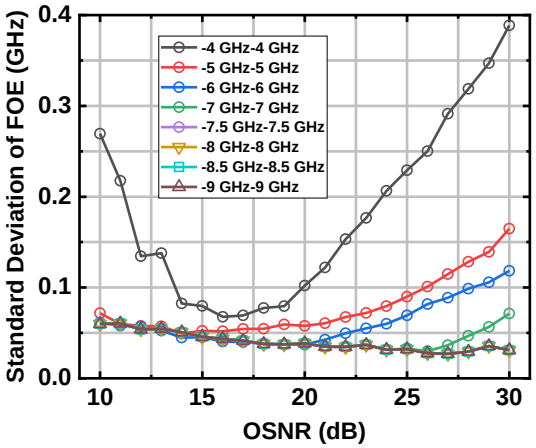

Fig. 7. Standard deviation of FOE versus OSNR with various FO sweeping range. The sweeping step size is 250 MHz and the Th is 0.4.

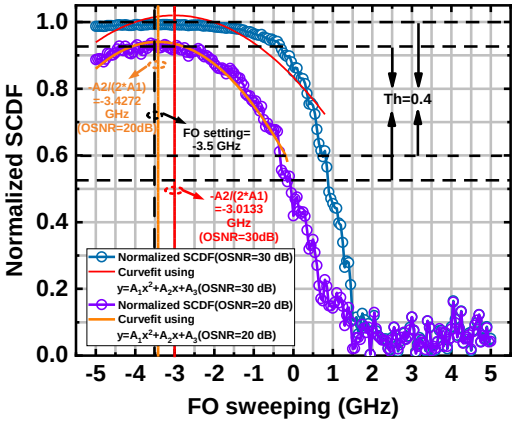

Fig. 8. An example case of FO estimation using quadratic function curve fitting method. The FO is set to -3.5 GHz. The FO sweeping range is [-5 GHz, +5 GHz].

range is reduced from $[-\alpha_0/8, +\alpha_0/8]$ to $[-\alpha_0/8q, +\alpha_0/8q]$. Here, the down-sampling rate q should satisfy $\alpha_0/8q > \max(abs(\text{coarse FOE error}))$, because the FOE range of fine FOE needs to be wide enough to cover the coarse FOE resolution. The maximum value of absolute coarse FOE error and the choice of down-sampling rate q will be discussed in Section IV.

IV. Optimization of FO Sweeping Range, Step Size, Threshold, and the Down-Sampling Rate

Theoretically, the FO sweeping range [-*Fs*/2, +*Fs*/2] can be arbitrary extended. Nevertheless, considering the practical requirement and complexity, it is better to choose a proper FO sweeping range. Here, we optimize the FO sweeping range to guarantee the FOE can functions well for a FO range of [-3.5 GHz, +3.5 GHz], which is also the FOE range of FFT-FOE for a 28 Gbaud signal. Figure 7 shows the relationship between standard deviation of FOE and OSNR with various FO sweeping range. In simulation, we use 16-QAM signal and the FO is arbitrarily set within the range of -3.5 GHz to 3.5 GHz. It can be seen that, when *Fs* is larger than or equal to 7.5 GHz, the standard deviation does not decrease anymore. Therefore, we fix the FO sweeping range at [-7.5 GHz, +7.5 GHz]. In Fig. 7, it can be observed that for insufficient FO sweeping range, the FOE performance usually deteriorates with OSNR. This

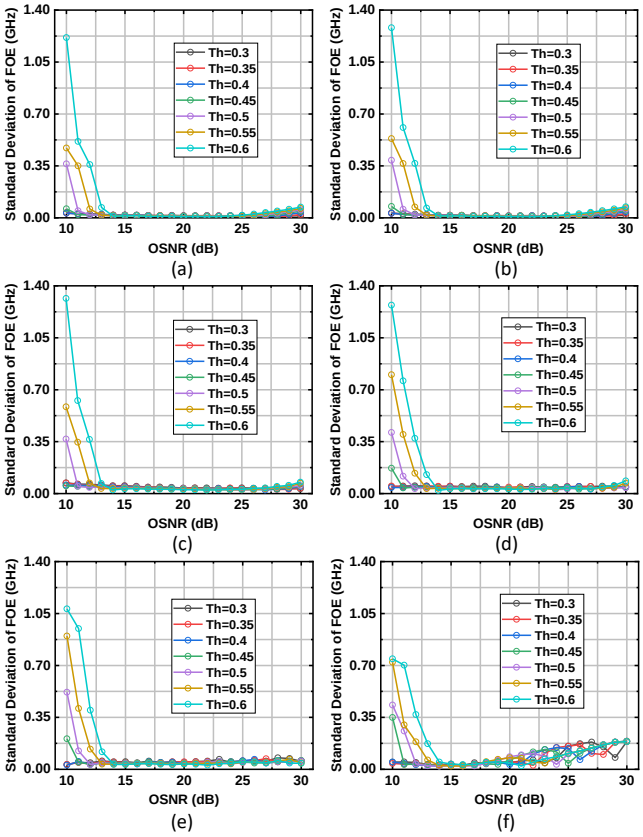

Fig. 9. Standard deviation of FOE versus OSNR with ΔF of (a) 50 MHz, (b) 100 MHz, (c) 250 MHz, (d) 500 MHz, (e) 1 GHz, and (f) 1.5 GHz.

abnormal phenomenon is due to the asymmetry of the data used for curve fitting. According to the analysis in Section II, we can conclude that the higher the OSNR is, the smaller the decline rate of $\hat{S}_m^{\alpha_0}(f)$ with FO is. As depicted in Fig. 8, the asymmetry of data used for curve fitting for OSNR of 30 dB is more severe than that for OSNR of 20 dB. Therefore, when the FO is large and the FO sweeping range is not wide enough, the performance of our proposed scheme will deteriarate with OSNR.

Next, we perform optimization of FO sweeping step size ΔF and the threshold (Th) for selection of data range for curve fitting. ΔF should be optimized considering the trade-off between FOE accuracy and complexity, while for different ΔF the optimized Th may be different. Figures 9(a)-9(f) plot the relationship between standard deviation of FOE and OSNR with ΔF of 50 MHz, 100 MHz, 250 MHz, 500 MHz, 1 GHz, and 1.5 GHz, respectively. It is observed that, even for ΔF of 1 GHz, the standard deviation of FOE can be relatively small and flat for OSNR ranging from 10 dB to 30 dB. Although FOE will be more accurate when ΔF is smaller than 1 GHz, the complexity increases. On the other hand, it should be noticed at this stage, only coarse FOC is required to guarantee the OSNR estimation performance. Therefore, we choose ΔF of 1 GHz (it means only 15 times FO sweeping is needed within [-7.5 GHz, +7.5 GHz]) and Th of 0.4 as the best parameters.

With above parameter optimizations, the standard deviation of FOE is less than 68 MHz. According to principle of normal distribution, the maximum absolute FOE value is almost

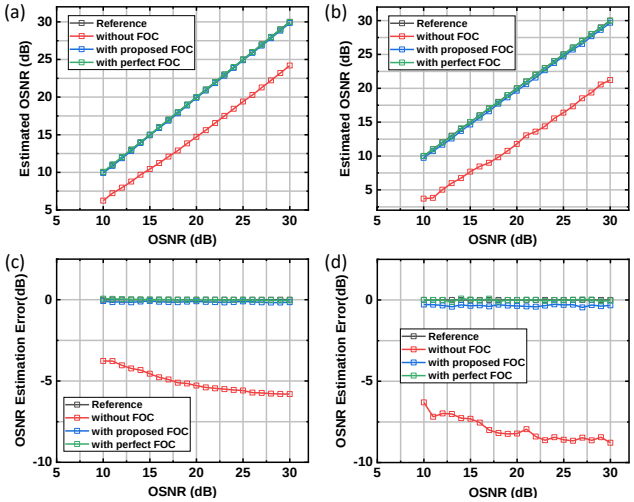

Fig. 10. OSNR monitoring performance using various FOC scheme for signal with ROF of (a) 0.5 and (b) 0.2; (c) OSNR estimation error in (a); (d) OSNR estimation error in (b).

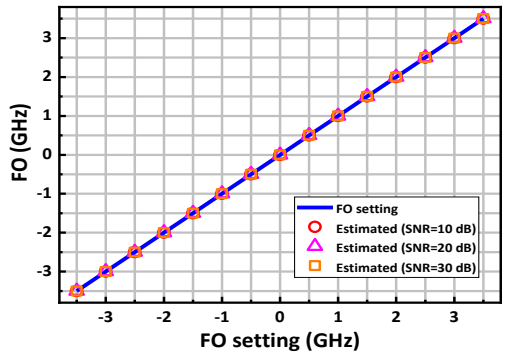

Fig. 11. FO estimation performance under SNR of 10 dB, 20 dB and 30 dB.

impossible to be greater than 3×68 MHz=204 MHz. For fine FOE stage with down-sampling, to guarantee the safety of fine FOE, we set that $\alpha_0/8q > 250$ MHz. Then, the q can be set to 14 for α_0=28 Gbaud.

V. Numerical Results of OSNR and FO Estimation

We carry out extensively simulation to evaluate OSNR estimation performance of our proposed scheme. OSNR of 28 GBaud 16-QAM with ROF of 0.5 or 0.2 is adjusted by adding additive white Gaussian noise (AWGN). FO is arbitrarily set within the range of -3.5 GHz to 3.5 GHz. For each OSNR calculation, we use 2^16-1 random symbols to acquire the OSNR estimation value. For each OSNR setting, 100 realizations are conducted to obtain an averaging estimation value. Figures 10(a) and 10(b) plot the curves of OSNR monitoring performance without FOC, with the proposed FOC and with the perfect FOC using known FO setting value for signal with ROF of 0.5 and 0.2, respectively. It can be clearly observed that, without FOC, the signal spectrum correlations-based OSNR monitoring scheme will underestimate the OSNR significantly, due to the impact of FO on the correlation values. On the contrary, with the proposed FOE and compensation, the estimated OSNR value matches reference OSNR very well. The OSNR estimation error curves are plotted in Fig. 10(c) and 10(d). For the proposed scheme it is shown that the absolute estimation error is lower than 0.18 dB and 0.46 dB for the signal with over the OSNR range of 10 dB to 30 dB. Then, we study the FO estimation performance for signal with ROF of 0.5 in Fig. 11. The FO is set from -3.5 GHz to +3.5 GHz and SNR is set to 10 dB, 20 dB, and 30 dB. As shown in Fig. 11, unbiased FO estimation is achieved by the proposed FO monitoring method. However, as discussed in Section IV, there still exists a certain degree of standard deviation of FOE. Either overestimation or underestimation of FO and corresponding FOC leads to an underestimation of OSNR. Therefore, it can be observed that the OSNR monitoring is not strictly unbiased estimation in Fig. 10. In contrast, the OSNR monitoring curve is slightly lower than the reference curve.

VI. Experiments Results

We carry out an optical back-to-back (B2B) experimental verification to further investigate the performance of our proposed joint OSNR and FO estimation scheme with a 28 Gbaud dual-polarization (DP)-4/16/32QAM coherent fiber optical transmission system which is illustrated in Fig. 12. Two external cavity lasers (ECLs) with ~100-kHz linewidth are used as the transmitter laser and LO. Here, various FOs can be set by adjusting the central wavelength of the ECL at

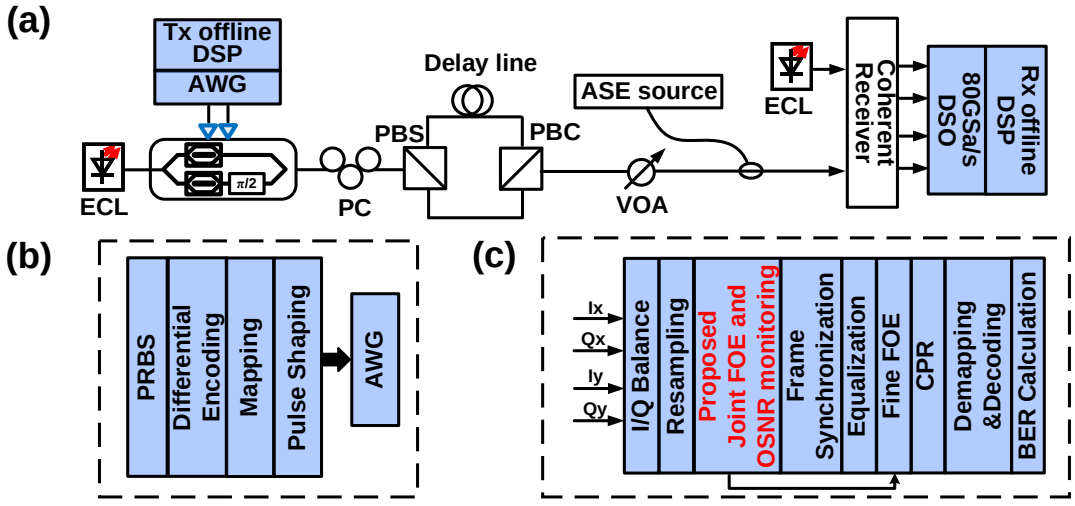

Fig. 12. (a) Experimental setup. (b) Tx DSP flow. (c) Rx DSP flow. (PC: polarization controller).

the receiver side (Rx). 28 Gbaud electrical signal is generated using an arbitrary waveform generator (AWG) and sent to an in-phase/quadrature (I/Q) modulator. Polarization division multiplexed is realized using polarization beam splitter (PBS), polarization beam combiner (PBC) and optical delay line between two polarization tributaries. For B2B measurements, the variable optical attenuator (VOA) and Erbium doped fiber amplifier (EDFA) based-ASE source are deployed to adjust the OSNR from 15 dB to 30 dB, which can be monitored by optical spectrum analyzer (OSA). After coherent detection, an 80 GSa/s digital sampling oscilloscope (DSO) is used to capture the electrical signal. For Rx offline processing DSP. The Tx and Rx DSP flows are shown in Fig. 12(b) and 12(c). At the Rx, after I/Q imbalance compensation and resampling to 2× sampling rate, the proposed joint OSNR and FO estimation scheme is operated with coarse FOC. Here, since only B2B transmission is conducted, there is no need for CDC. However, if the signal is transmitted over an optical fiber link, CD estimation [28] and corresponding CDC in frequency domain [29] are compulsory to guarantee the OSNR and FO monitoring performance. Adaptive equalization is realized using four 15-taps fractionally-spaced (Ts/2) finite impulse-response (FIR) filters with two-stage structure consisting of standard constant modulus algorithm (CMA) and radius-directed equalization (RDE) algorithm. Then, for fine FOE, the proposed down-sampling process based FFT-FOE is employed, while the conventional FFT-FOE is used as reference. After blind phase searching (BPS)-based CPR, de-mapping and decoding, BER is calculated for performance evaluation [17].

Figures 13(a)-13(c) show OSNR monitoring performance for 4-/16-/32-QAM, respectively. In our experiment, the FO is adjusted to three values of 0 GHz, -2 GHz, and +2 GHz. We choose the FO of -2 GHz, 0 GHz, and +2 GHz to investigate the FOE performance under the large negative condition, small condition, and large positive condition of FO. With the proposed scheme, the OSNR monitoring performs well for all FO settings. Thanks to the DSP-induced penalty-free feature, the proposed scheme shows satisfactory monitoring performance for a wide OSNR range. The absolute estimation error is lower than 0.51 dB, 0.66 dB, and 0.65 dB for OSNR ranging from 15 dB to 30 dB for 4-/16-/32-QAM, respectively. However, for the scheme without FOC, the estimated OSNR value is severely underestimated. The BER performance curves of DP-16-QAM for FO setting at 0 GHz, -2 GHz, and +2 GHz are plotted in Fig. 14. It indicates that the performance of the proposed down-sampling process based FFT-FOE is the same as that of conventional FFT-FOE, while the complexity is reduced by down-sampling process. It is observed that the estimated OSNR curve fluctuates without FOC. It can be explained by the reason that if the FO is not well compensated, the OSNR estimation is severely disturbed and there is no definite relation between the estimation penalty and FO. Therefore, for the OSNR estimation without FOC, there arises fluctuations while for the estimation with FOC, the performance is more stable. For conventional FFT-FOE without a prior coarse FOC, the block size N of FFT-FOE is set to 1008, resulting the FOE resolution of 28 GHz/4/1008=6.94 MHz. The number of required real multipliers and real adders for FFT-FOE are

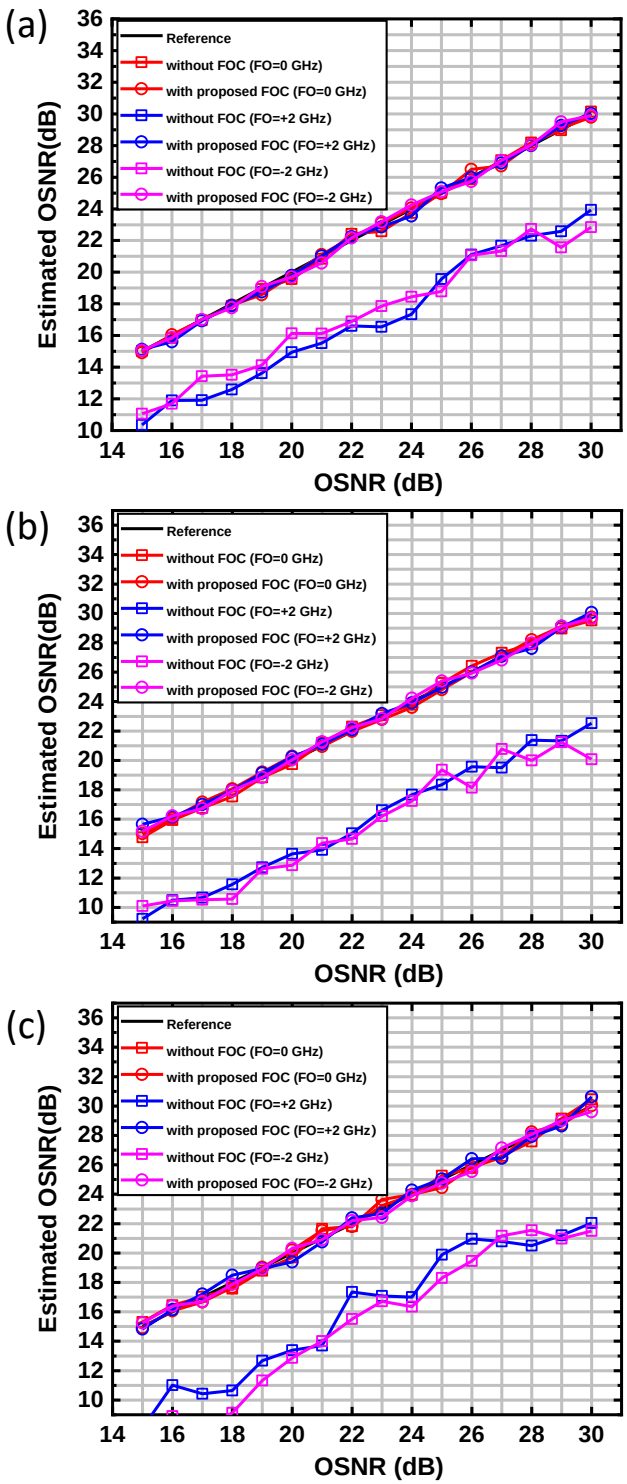

Fig. 13. OSNR monitoring performance for (a)4-QAM, (b)16-QAM, and 32-QAM with various FOC schemes.

$2N\log_2 N+10N+2$=30196 and $3N\log_2 N+5N$=35211, respectively [30]. For down-sampling process based FFT-FOE, the signal is down sampled by q=14, reducing the required FFT size to 1008/14=72. Then, the number of required real multipliers and real adders for are only 1610 and 1693, respectively, while the FOE resolution of down-sampling process based FFT-FOE is the same as that of conventional FFT-FOE. Therefore, in Fig. 14, both FOE methods show

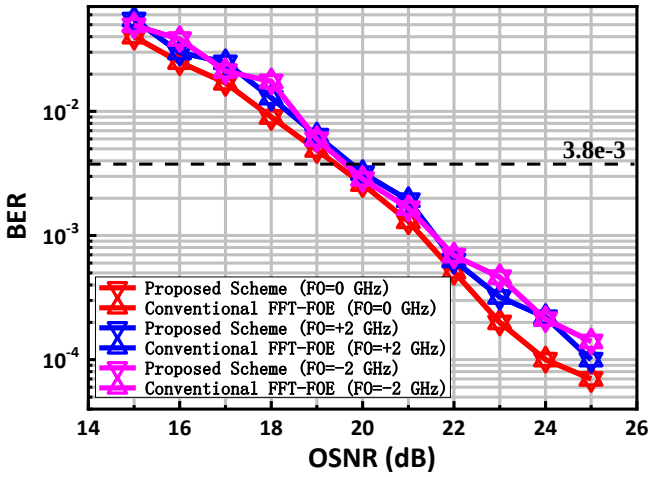

Fig. 14. BER versus OSNR using proposed down-sampling based FFT-FOE and conventional FFT-FOE with various FO setting.

similar performance, indicating our proposed scheme functions well for various FO conditions.

In this paper, we do not study the robustness of the proposed scheme to fiber nonlinearity. However, as an important factor in fiber optical communication systems, fiber nonlinearity is expected to damage the OSNR monitoring performance since the nonlinear noise can be modeled as a Gaussian-like noise which will affect the correlation value. On the other hand, the coarse FO estimation is expected to suffer less from fiber nonlinearity since it is obtained from curve fitting using quadratic function rather than the absolute correlation values. The scheme to improve the robustness to fiber nonlinearity is left for future study.

VII. Conclusions

An efficient and modulation-format-transparent joint OSNR and FO estimation scheme is proposed for coherent optical fiber communication systems. By FO sweeping, correlation value calculation and quadratic function-based curve fitting, a coarse FOC can be performed to guarantee accurate OSNR estimation and to reduce the complexity of fine FOE stage. The performance of our proposed scheme is numerically and experimentally verified with low OSNR estimation error and reliable FOE performance.

References

[1] K. Roberts, Q. Zhuge, I. Monga, S. Gareau, and C. Laperle, "Beyond 100 Gb/s: Capacity, flexibility, and network optimization," *IEEE Commun. Lett.* vol. 9, no.4, pp. C12-C24, 2017.

[2] Z. Dong, F. N. Khan, Q. Sui, K. Zhong, C. Lu, and A. P. T. Lau, "Optical performance monitoring: A preview of current and future technologies," *J. Lightw. Technol.*, vol. 34, no.2, pp. 525-543, Sep. 2016.

[3] W. Shieh, R. S. Tucker, W. Chen, X. Yi, and G. Pendock, "Optical performance monitoring in coherent optical OFDM systems," *Opt. Express*, vol. 15, no. 2, pp. 350–356, 2007.

[4] J. Zhao, L. Gan, L. Su, J. Zhang, H. He, W. Cai, J. Wang, S. Fu and M. Tang, "Carrier Beating Impairment in Weakly Coupled Multicore Fiber-Based IM/DD Systems," *IEEE Access*, vol. 8, no. 1, pp. 65699–65710, 2020.

[5] Q. Zhuge , X. Zeng , H. Lun, M. Cai, X. Liu , L. Yi , and W. Hu, "Application of Machine Learning in Fiber Nonlinearity Modeling and Monitoring for Elastic Optical Networks," *J. Lightw. Technol.*, vol. 37, no.13, pp. 3055-3063, Apr. 2019.

[6] D. C. Kilper, S. Chandrasekhar, L. Buhl, A. Agarwal, and D. Maywar, "Spectral monitoring of OSNR in high speed networks," in *European Conference and Exhibition on Optical Communication* (ECOC), 2002, paper 7.4.4.

[7] W. Jin, C. Zhang, X. Zhang, X. Duan, Y. Dong, R. Giddings, K. Qiu, and J. Tang, "OSNR penalty-free add/drop performance of DSP-enabled ROADMs in coherent systems," *Opt. Commun. Netw*. vol. 9, no. 9, pp. 730–738, 2017.

[8] S. J. Savory, "Digital filters for coherent optical receivers," *Opt. Express*, vol. 16, no. 2, pp. 804–817, 2008.

[9] R. Schmogrow, B. Nebendahl, M. Winter, A. Josten, D. Hillerkuss, S. Koenig, J. Meyer, M. Dreschmann, M. Huebner, C. Koos, J. Becker, W. Freude, and J. Leuthold, "Error vector magnitude as a performance measure for advanced modulation formats," *IEEE Photon. Technol. Lett.*, vol. 24, no. 1, pp. 61–63, Oct. 2012.

[10] T. Saida, I. Ogawa, T. Mizuno, K. Sano, H. Fukuyama, Y. Muramoto, Y. Hashizume, H. Nosaka, S. Yamamoto, and K. Murata, "In-band OSNR monitor with high-speed integrated Stokes polarimeter for polarization division multiplexed signal," *Opt. Express*, vol. 20, pp. B165–B170, 2012.

[11] C. Zhu, A. Tran, S. Chen, L. Du, C. Do, Trevor Anderson, Arthur J. Lowery, and Efstratios Skafidas, "Statistical moments-based OSNR monitoring for coherent optical systems," *Opt. Express*, vol. 20, no. 16, pp. 17711–17721, 2012.

[12] M. Ionescu, M. Sato, and B. Thomsen, "Cyclostationarity based joint monitoring of symbol-rate, frequency offset, CD and OSNR for Nyquist WDM superchannels," *Opt. Express*, vol. 23, no. 20, pp. 25762–25772, 2015.

[13] F. L. Heismann, "Determining in-band optical signal-to-noise ratio in polarization-multiplexed optical signals using signal correlations", U.S. Patent US 2018/0138974 Al, 2018.

[14] J. Lu, and C. Lu, "Frequency offset drift monitoring: enabling simultaneously optimum performance and minimum cost of frequency offset estimation," *Opt. Lett.*, vol. 44, no. 15, pp. 3753-3756, 2019.

[15] M. Selmi, Y. Jaou¨en, P. Ciblat, and B. Lankl, "Accurate digital frequency offset estimator for coherent PolMux QAM transmission systems," in *European Conference and Exhibition on Optical Communication* (ECOC), 2009.

[16] A. Meiyappan, P. Kam, and H. Kim, "On decision aided carrier phase and frequency offset estimation in coherent optical receivers," *J. Lightw. Technol.*, vol. 31, no.13, pp. 2055-2069, Jul. 2013.

[17] J. Lu, X. Li, S. Fu, M. Luo, M. Xiang, H. Zhou, M. Tang, and D. Liu, "Joint carrier phase and frequency-offset estimation with parallel implementation for dual-polarization coherent receiver," *Opt. Express*, vol. 25, no. 5, pp. 5217-5231, 2017.

[18] M. Y. Sowailem, T. M. Hoang, M. Morsy-Osman, M. Chagnon, M. Qiu, S. Paquet, C. Paquet, I. Woods, Q. Zhuge, O. Liboiron-Ladouceur, and D. V. Plant, "770-Gb/s PDM-32QAM coherent transmission using InP dual polarization IQ modulator," *IEEE Photon. Technol. Lett.* 29, pp. 442–445, Jan. 2017.

[19] M. Qiu, Q. Zhuge, M. Chagnon, Y. Gao, X. Xu, M. Morsy-Osman, and D. V. Plant, "Digital subcarrier multiplexing for fiber nonlinearity mitigation in coherent optical communication systems," *Opt. Express*, vol. 22, no. 15, pp. 18770–18777, Jul. 2014.

[20] H. Sun et al., "800G DSP ASIC Design Using Probabilistic Shaping and Digital Sub-Carrier Multiplexing," *J. Lightw. Technol.*, vol. 38, no. 17, pp. 4744 – 4756, Sept. 2020.

[21] Z. Xiao, S. Fu, S. Yao, M. Tang, P. Shum and D. Liu, "ICI Mitigation for Dual-Carrier Superchannel Transmission Based on m-PSK and m-QAM Formats," *J. Lightw. Technol.*, vol. 34, no.23, pp. 5526-5533, Dec. 2016.

[22] M. Ionescu, "Digital Signal Processing for Sensing in Software Defined Optical Networks", PhD's thesis, the University College London, 2015.

[23] W. A. Gardner, A. Napolitano, and L. Paura, "Cyclostationarity: Half a century of research", *Signal Process*., vol. 86, no. 4, pp. 639–697, 2006.

[24] J. Lu, S. Fu, M. Tang, M. Xiang, P. Shum, and D. Liu, "Low-complexity carrier phase estimation for M-ary QAM based on blind phase search using simplified measurement," in *Proc. Int. Conf. Opt. Commun. Netw*., pp. 1–3, 2016.

[25] M. S. Faruk, Y. Mori, and K. Kikuchi, "In-Band estimation of optical signal-to-noise ratio from equalized signals in digital coherent receivers," *IEEE Photon. J.*, vol. 6, no. 1, p. 7800109, Feb. 2014.

[26] X. Lin, O. A. Dobre, T. M. Ngatched, and C. Li, "A non-data-aided OSNR estimation algorithm for coherent optical fiber communication systems employing multilevel constellations," *J. Lightw. Technol.*, vol. 37, no. 15, pp. 3815–3825, Aug. 2019.

[27] J. Lu, Q. Wu, H. Jiang, S. Fu, M. Tang, and C. Lu, "Efficient Timing/Frequency Synchronization Based on Sparse Fast Fourier Transform (S-FFT)," *J. Lightw. Technol.*, vol. 37, no.20, pp. 5299-5308, Oct. 2019.

[28] R. A. Soriano, F. N. Hauske, N. G. Gonzalez, Z. Zhuhong, Y. Yabin, and I. T. Monroy, "Chromatic dispersion estimation in digital coherent receivers," *J. Lightw. Technol.*, vol. 29, no. 11, pp. 1627–1637, Jun. 2011.
[29] B. S. G. Pillai, B. Sedighi, W. Shieh, and R. S. Tucker, "Chromatic dispersion compensation—An energy consumption perspective," in Proc. Opt. Fiber Commun. Conf., Los Angeles, CA, USA, Mar. 2012, pp. 1–3
[30] J. Lu, Y. Tian, S. Fu , X. Li, M. Luo, M. Tang, and D. Liu., "Frequency offset estimation for 32-QAM based on constellation rotation," *IEEE Photon. Technol. Lett.*, vol. 29, no. 23, pp. 2115–2118, Dec. 2017.

Jing Zhou was born in Beijing, China, in 1993. He received the B. Eng. degrees in optical and electrical information engineering in 2016 from Huazhong University of Science and Technology, Wuhan, China. He is currently working toward the M.Sc. degree in Photonics Research Centre, Department of Electronic and Information Engineering, The Hong Kong Polytechnic University, Hong Kong. His research is focused on digital coherent optical communication and optical performance monitoring.

Jianing Lu was born in Zhejiang Province, China, in 1993. He received the B. Eng. and the M. Eng. degrees in optical and electrical information engineering, in 2015 and 2018, from Huazhong University of Science and Technology, Wuhan, China. From June 2017 to January 2018, he was a Research Associate with the Department of Information Engineering, Chinese University of Hong Kong. He is currently working toward the Ph.D. degree in Photonics Research Centre, Department of Electronic and Information Engineering, The Hong Kong Polytechnic University, Hong Kong. His research is focused on digital coherent optical communication, optical performance monitoring and digital signal processing algorithms.

Gai Zhou received the B.S. degree from South China Normal university, Guangzhou, in 2015. He is currently working toward the Ph. D degree in optical communication engineering at the Hong Kong Polytechnic University, Kowloon, Hong Kong. His current research interests include DSP in optical transmission system and nonlinear frequency division multiplexing systems for fiber communication.

Chao Lu received the B.Eng. degree in electronic engineering from Tsinghua University, China in 1985, and the M.Sc. and Ph.D. degrees from the University of Manchester, Manchester, U.K., in 1987 and 1990 respectively. He joined the School of Electrical and Electronic Engineering, Nanyang Technological University (NTU), Singapore in 1991 and worked there as a Lecturer, Senior Lecturer, and Associate Professor until 2006. From June 2002 to December 2005, he was seconded to the Institute for Infocomm Research, Agency for Science, Technology and Research (A∗STAR), Singapore, as the Program Director and Department Manager leading a research group in the area of optical communication and fiber devices. He joined the Department of Electronic and Information Engineering, The Hong Kong Polytechnic University, Kowloon, Hong Kong, as a Professor in 2006 and is currently Chair Professor of Fiber Optics. Over the years, he has published more than 300 papers in major international journals. He has been organizer or technical program committee member of many international conferences. His current research interests include high capacity transmission techniques for long haul and short reach optical systems and optical sensing systems. He is a Fellow of the Optical Society (OSA).